WILEY-VCH

DOI: 10.1002/ ((please add manuscript number))
Article type: Full Paper

Nonvolatile All-optical 1x2 Switch for Chipscale Photonic Networks

*Matthias Stegmaier, Carlos Ríos, Harish Bhaskaran, C. David Wright, Wolfram H.P. Pernice**

Carlos Ríos, Prof. Harish Bhaskaran
Department of Materials, University of Oxford, Parks Road, Oxford OX1 3PH, UK

Prof. David Wright
Department of Engineering, University of Exeter, Exeter, EX4 QF, UK

Matthias Stegmaier, Prof. Wolfram H.P. Pernice
Institute of Physics, University of Münster, 48149 Münster, Germany
E-Mail: wolfram.pernice@uni-muenster.de

Keywords: all-optical switching, hybrid nanophotonic circuits, phase-change materials

Integrated chip-level photonics has the potential to revolutionize future computer systems by eliminating the “von-Neumann information bottleneck” and the power losses resulting from the use of electrical interconnects. Yet the need for optical-to-electrical conversion has so far hindered the implementation of chip-level all-optical routing schemes which remain operational without continuous power consumption. Here we demonstrate a crucial component to successful implementation of such all-photonic networks - an effective, practicable all-optical nonvolatile switch. Current integrated all-optical switches require constant bias power to operate, and lose their state when it is removed. In contrast, our switch is entirely nonvolatile, with the direction of light flow altered by switching the phase state of an embedded phase-change cell using 1 ps optical pulses. We achieve high on/off switching contrast devices that are fully integrated and compatible with existing photonic circuits. We show that individual switching events occur with transition times below 200 ps and thus hold promise for ultra-fast light routing on chip. Our approach offers a reliable and simple route towards hybrid reconfigurable photonic devices without the need for electrical contacting.

1. Introduction

Optical data communication is the most viable solution to overcoming the bandwidth limitations of conventional electronic signaling. While in the past light has been used predominantly for long-distance information transfer, rapid progress in the fabrication of on-chip photonic circuits has now paved the way for optical telecommunication between single chips[1], even down to the on-chip level[2]. Such chip-chip and intra-chip photonic communication offers great promise for eliminating the major performance limitation of modern computer systems, that of moving data to and from the CPU and system memory (the von-Neumann bottleneck)[3,4]. In photonic telecommunication systems active components such as modulators and switches are essential to control the light flow within the network. Such devices typically control the refractive index within an interferometer or a cavity by electrical[5], optical[6] or acoustical[7] means or employ plasmonic effects[8]. Since purely optical networks promise higher operational speeds, all-optical routing devices are of particular interest. In particular, optical bistabilities in photonic crystal cavities show promise for high-rate, low-power bit-by-bit switching of optical signals[9,10]. However, all such devices reported thus far require a steady optical bias to keep their current state. Although this bias power is notionally negligible in high-rate bit-by-bit switching, it severely limits the energy consumption in routing schemes where switching occurs at much lower frequencies than the actual data rate, e.g. packet-switching[11].

Recently, phase-change materials (PCMs) have emerged as promising candidates to provide non-volatility for on-chip all-optical operations[12–14]. Because of the high refractive index contrast between their amorphous and crystalline state they enable high on-off ratio and wide tunability in photonic components[15]. The transition between these phases is typically triggered by appropriate heat-stimuli[16] which can be supplied by short optical pulses. PCMs

feature a multitude of intriguing properties such as high switching contrast in both the optical and electronic domain, phase transition times down to sub-nanoseconds[17], data retention for years and high cyclability up to 10^{12} switching cycles[18], which makes them highly attractive for nonvolatile applications, exploited in particular to date in memory devices[16,18]. In addition, the optical and electrical properties of PCMs have been demonstrated to enable so-called mixed-mode application[19] where the PCM is switched electrically affecting the optical domain or vice versa.

Here, we demonstrate an on-chip nonvolatile all-optical switch based on the PCM $Ge_2Sb_2Te_5$ (GST). The device does not require constant power supply to keep its state, in contrast to previously reported all-optical switches. Furthermore, it is fully-integrated such that it can be easily combined with other on-chip photonic circuitry.

2. Device principle

The operation principle of our all-optical switch is presented in **Figure 1**. The device, as shown in Figure 1a, consists of a nanoscale GST element on top of an on-chip ring resonator that is evanescently coupled to two waveguides. Probe light with off-resonance wavelength is directed to the "THROUGH" port, cf. Figure 1b, while on-resonance light is partially coupled into the ring and exits from there into the "DROP" port. The ratio of power coupled to the DROP and THROUGH port depends on the coupling and attenuation parameters of the ring cavity. For light with on-resonance wavelength (orange marker in Figure 1b) the direction of the light flow can thus be changed by adjusting one of these two parameters. Here, we predominantly change the attenuation within the cavity by switching the GST between its low-loss amorphous and highly absorptive crystalline state. Evanescent interaction between the guided mode and the GST directly influences the electromagnetic phase and the amplitude of the intra-cavity light[20]. The phase transformations of the GST element, amorphization and crystallization, are initiated with 1 ps optical Write pulses (red marker in Figure 1b) which are also sent into the device via

the on-chip photonic circuitry. Since the spatial length of these optical pulses is shorter than the cavity itself, intra-cavity interference does not take place. Therefore, the amount of optical power coupled into the ring does not change when the wavelength of the picosecond pulse is on or off-resonance.

3. Results

We control the direction of the light flow in our device by switching the GST between the amorphous and crystalline phase state. The transmission spectra of the device in these two states are presented in **Figure 2**. In the highly-absorptive crystalline state (black trace) the loss within the ring resonator exceeds the coupling loss to the waveguide[21]. In this weakly-coupled regime, the resonance dip observed in the THROUGH port (upper panel) has a relatively broad full width half maximum (FWHM) of 1.18 nm (corresponding to a Q-factor of 1300) and a moderate extinction ratio of 4.3 dB. Upon amorphization (red trace), the attenuation within the cavity decreases drastically (by about 3 dB) resulting in both a more narrow (FWHM of 0.69 nm, thus Q-factor of 2400) and a deeper (extinction ratio of 9.7 dB) resonance. This drastic change in the resonance shape is due to the fact that now the loss within the cavity matches the coupling loss, i.e. the ring is designed to be critically coupled in the low-loss amorphous state. The resonance dip observed in the DROP port (lower panel) shows the same behavior. While in the crystalline state, due to high attenuation of the intra-cavity light, the height of the resonance is relatively small (-11 dB peak transmission) it considerably increases upon amorphization (-5.1 dB peak transmission). Therefore, light with on-resonance wavelength (here 1562.3 nm) is directed to the THROUGH/ DROP port with an insertion loss of -4.3/ -5.1 dB by setting the GST in its crystalline/ amorphous state. The on-off switching contrast exceeds 5 dB in both ports.

All-optical operation of the switch is presented in **Figure 3**. The device is probed with 500 ps optical pulses with 2.5 pJ energy and with on-resonance wavelength to achieve maximum on/off switching contrast. Three identical probe pulses are sent into the device (Figure 3a, black trace) separated by an amorphization (I) and crystallization (II) event. In the initial (crystalline) state most of the light is directed to the THROUGH port (central, blue trace). Amorphization (I) of the GST, however, results in a redirection of the light flow to the DROP port (lower, green trace): The optical power transmitted to the DROP port increases by 4.9 dB while the respective power sent into the THROUGH port decreases by 4.7 dB. The subsequent crystallization (II) of the GST recovers the initial state. This measurement with 500 ps pulses demonstrates that packet with bit rates exceeding 1 Gb/s can be routed with our nonvolatile switch. However, due to a photon lifetime of approximately 2 ps, derived from the quality factor of the ring in the amorphous state, we expect that considerably higher bit rates (exceeding 100 Gb/s) should be possible.

As sketched in the upper panel of Figure 3b, for amorphization we use two 1 ps pulses of 95 pJ energy (separated by 25 ns, given by the repetition rate of the pulsed laser). This two-step amorphization scheme enables high switching contrast and avoids any possible damage to the GST layer. The reason for the latter is the strong exponential decay of the optical field along the cell due to the high absorption coefficient of crystalline GST. Thus, a single amorphization pulse strong enough to amorphize the back end of the cell can easily damage its front end. In contrast, crystallization is induced stepwise by a train of pulses with decreasing energy, ranging from 38 pJ down to 19 pJ, as shown in the lower panel of Figure 3b. The pulses are grouped into sequences of 100 pulses each with a fixed repetition time of 25 ns between consecutive pulses.

We monitor the transient behavior of the all-optical switch upon amorphization with an ultra-fast 12 GHz photodetector (New Focus, Model 1554B) and a 6 GHz oscilloscope (Agilent

Infiniium 54855A). The transmitted light is first sent through a fiber-coupled optical bandpass filter (Pritel, TFA-1550) to suppress the transmitted pump power. Afterwards the signal is amplified by an erbium-doped fiber amplifier to increase the signal-to-noise ratio encountered at the photodetector. Finally, the signal is again filtered to further suppress the pump power and to remove unwanted amplifier noise. The resulting signal of the THROUGH port is plotted in Figure 3c for on- resonance probe wavelength and a switching event occurring at time delay 0 s. Overall, the signal drops within a few hundred picoseconds to a lower transmission level, as expected from an amorphization event. Since this transition takes place within less than 200 ps we expect our measurement to be limited by the timing resolution of the oscilloscope used (6 GHz), in consistency with reported amorphization times of tens of picoseconds[22]. Nevertheless, this measurement demonstrates that our switch can be closed on a sub-nanosecond timescale. Furthermore, we note that thermo-optical effects, which have been shown to relax within ~1 ns[14], do not limit the switching time. This is because the thermo-optical contributions to the real and complex part of the refractive index cancel each other out at wavelengths close to resonance. The initial increase of the signal at time t = 0 is due to free-carrier effects[22,23] and a not completely suppressed pump pulse (whose power exceeds the probe power by 7 orders of magnitude).

Finally, we demonstrate high reproducibility of the all-optical operation of our device. In **Figure 4a** the transmitted power at the THROUGH port is plotted upon completing 10 full switching cycles. Each switching cycle consists, as explained in Figure 3b, of one amorphization step (two 1 ps pulses) and six crystallization steps (100 picosecond pulses each). As can be seen from the observed transmission values, our switching scheme allows highly reproducible operation between the on- and off state. Furthermore, the data suggests that similarly to our previous results[14], intermediate states can also reliably be accessed. We have further carried out successive operation up to 1000 cycles, as shown in Figure 4b, without

considerable reduction in switching contrast. Here, contrast is defined as the ratio of the transmitted powers in the two states. We observe a conditioning process within the first few switching cycles during which the reproducibility of the device operation stabilizes.

4. Discussion

Our results demonstrate that a single picosecond laser source with adjustable output power is sufficient to reliably redirect the light flow within the presented nonvolatile all-optical switch, i.e. to induce both amorphization and crystallization. The 1 ps pulses employed in our experiments simplify device operation because matching of the laser wavelength to a cavity resonance is not required. This is in particular interesting for cavities which exhibit a considerable resonance shift upon switching.

The demonstrated accumulated switching times of 25 ns (amorphization) and 15 µs (crystallization) can be significantly reduced by increasing the repetition rate of the ps-laser system (here 40 MHz). By doing so, our two-step amorphization scheme can be carried out on a sub-nanosecond timescale due to the fast 200 ps transition time of a single event (Figure 3c). In contrast, the crystallization time can be reduced to the nanosecond regime. Here, the high number of pulses is necessary since the heat generated by a single picosecond pulse diffuses away too fast to induce more than a small partial recrystallization of the GST-cell[24]. However, proper heat-management within the device might enable even single-shot crystallization with picosecond pulses[25].

The switching contrast of the all-optical switch can be further improved by using a larger GST cell and/or a smaller cavity size. The former might require, as explained earlier, more than two amorphization pulses to avoid cell degradation. In contrast, smaller cavities are more sensitive to the real part of the refractive index of the PCM-cell which results in a more pronounced shift of the resonance wavelength upon switching. Since the probing is performed

at a single wavelength, this shift can dramatically increase the switching contrast. In particular in high refractive index materials like silicon, high-Q ring resonators can be fabricated with small cavity size (ring radii down to a few μm[26]). Furthermore, small mode volume can be achieved in photonic crystal cavities regardless of the material.

A major benefit of our device here is its non-volatility - once set into a state no further power supply is required to maintain that state. To the best of our knowledge, this is the first fully-integrated on-chip all-optical switch with this property. Our switching scheme requires accumulated 180 pJ and 17 nJ of pulse energy to induce amorphization and crystallization, respectively. In particular the energy for crystallization can in the future significantly be reduced by using longer pulses or higher repetition rates to enable efficient heat accumulation within the cell during the pulse sequence. Both of these energies can be reduced by using longer (at least a few picoseconds) pulses with on-resonance wavelength which are more efficiently absorbed by the PCM-cell. In accordance with our previous results, we expect that switching energies down to tens of pJ are possible[14]. In comparison, all-optical volatile switches have been demonstrated to consume just a few fJ/bit[10]. However, they also require a bias power of typically a few μW to keep a state after switching. Therefore, in applications with relatively low-rate switching operation, such as packet-switching or reconfigurable on-chip and chip-chip routing, our nonvolatile device enables considerable lower overall power consumption while still supporting prospective bit-rates up to 100 Gb/s.

5. Conclusion

We have demonstrated, for the very first time, that phase-change materials can be used in an on-chip photonic cavity to reliably operate a nonvolatile all-optical 1x2 switch with a single 1 ps laser source. Within the device the light-flow is directed to one of two ports with low insertion loss and high switching contrast in both ports. Transition times of less than 200 ps

hold promise for ultra-fast, down to sub-nanosecond, switching times. Since, in contrast to previously reported all-optical switches, the device keeps its state after switching without an optical bias power, it offers significant lower power consumption for all-optical packet-switching, routing to multi-core architectures and reconfigurable on-chip photonic networks. Therefore, these results hold promise for future on-chip all-optical networks for high-speed data communication.

6. Experimental Section

Fiber-optic setup:

The on-chip device is characterized with an off-chip optical fiber setup. Light is coupled into and out of the chip with focusing grating couplers which are optimized for light around 1550 nm. The transmission spectra are recorded with a tunable continuous wave (CW) laser (Santec, TSL-510C) in combination with low-noise photodetectors (New Focus, Model 2011). For pulsed probing of the device 500 ps pulses are generated from the CW laser with an electro-optical modulator (Lucent Technologies, 2623CS) which is controlled by a 500 MHz electrical pulse generator (HP 8131A). The GST is switched with a fiber-coupled femtosecond laser source which emits 1 ps optical pulses at a repetition rate of 40 MHz (Pritel, FFT). A homemade pulse picker, an acousto-optical modulator (Gooch & Housego, Fiber-Q T-M040) connected to a 500 MHz electrical pulse generator (HP 8131A), is used to control the pulse sequence sent into the device. The pulse generator, which is synchronized to the mode-locked fiber laser via its trigger input, enables precise control of the opening level and opening time of the acousto-optical modulator and thus the pulse number and pulse power. Before the pulses are sent into the device they are further amplified with an erbium-doped fiber amplifier (Pritel, LNHPFA-33).

Device fabrication:

Our device is fabricated in a multi-step electron-beam lithography procedure[27] followed by GST sputter deposition and lift-off[28]. First, the photonic circuits are fabricated from a 330 nm thick silicon nitride-on-insulator layer using electron-beam lithography and subsequent dry etching. The waveguides are fully etched down to the oxide buffer layer and have a designed width of 1.1 µm. The ring has a radius of 30 µm and the gaps between the ring and the waveguides are designed to be 150 nm and 200 nm for the lower and upper gap (see Figure 1b), respectively. This imbalance between the two gaps results in critical coupling in the amorphous phase-state[21]. After dry etching, opening windows with a footprint of 600x750 nm^2 for the PCM-sections are defined on top of the waveguides in a further lithography step with positive tone Polymethylmethacrylat (PMMA) resist. Subsequently, 20 nm of GST and 10 nm of indium tin oxide (ITO) are sputter deposited and lift-off. The ITO is used to cap the GST in order to prevent oxidation. Eventually, the chip is placed for 10 min on a hotplate at 200 °C to crystallize the as-deposited amorphous GST.

Acknowledgements

We acknowledge support by DFG grant PE 1832/1-1 and PE 1832/2-1 and EPSRC grants EP/J018783/1, EP/M015173/1 and EP/M015130/1. C.R. is grateful to Clarendon Fund for funding his graduate studies. M. S. acknowledges support by the Karlsruhe School of Optics and Photonics (KSOP) and the Stiftung der Deutschen Wirtschaft (sdw). The authors thank S. Diewald for assistance in device fabrication, M. Blaicher for technical assistance in device design and A. Vetter and P. Rath for helpful discussions

Received: ((will be filled in by the editorial staff))
Revised: ((will be filled in by the editorial staff))
Published online: ((will be filled in by the editorial staff))

References

[1] M. Paniccia, *Nat. Photonics* **2010**, *4*, 498.

[2] C. Sun, M. T. Wade, Y. Lee, J. S. Orcutt, L. Alloatti, M. S. Georgas, A. S. Waterman, J. M. Shainline, R. R. Avizienis, S. Lin, B. R. Moss, R. Kumar, F. Pavanello, A. H. Atabaki, H. M. Cook, A. J. Ou, J. C. Leu, Y.-H. Chen, K. Asanović, R. J. Ram, M. A. Popović, V. M. Stojanović, *Nature* **2015**, *528*, 534.

[3] A. Alduino, M. Paniccia, *Nat. Photonics* **2007**, *1*, 153.

[4] R. Kirchain, L. Kimerling, *Nat. Photonics* **2007**, *1*, 303.

[5] G. Reed, G. Mashanovich, F. Gardes, D. Thomson, *Nat. Photonics* **2010**, *4*, 518.

[6] V. R. Almeida, C. A. Barrios, R. R. Panepucci, M. Lipson, *Nature* **2004**, *431*, 1081.

[7] S. A. Tadesse, M. Li, *Nat. Commun.* **2014**, *5*, 5402.

[8] C. Hoessbacher, Y. Fedoryshyn, A. Emboras, A. Melikyan, M. Kohl, D. Hillerkuss, C. Hafner, J. Leuthold, *Optica* **2014**, *1*, 198.

[9] K. Nozaki, T. Tanabe, A. Shinya, S. Matsuo, T. Sato, H. Taniyama, M. Notomi, *Nat. Photonics* **2010**, *4*, 477.

[10] K. Nozaki, A. Shinya, S. Matsuo, Y. Suzaki, T. Segawa, T. Sato, Y. Kawaguchi, R. Takahashi, M. Notomi, *Nat. Photonics* **2012**, *6*, 248.

[11] K. Nozaki, A. Lacraz, A. Shinya, S. Matsuo, T. Sato, K. Takeda, E. Kuramochi, M. Notomi, *Opt. Express* **2015**, *23*, 30379.

[12] D. Tanaka, Y. Shoji, M. Kuwahara, X. Wang, K. Kintaka, H. Kawashima, T. Toyosaki, Y. Ikuma, H. Tsuda, *Opt. Express* **2012**, *20*, 442.

[13] M. Rudé, J. Pello, R. E. Simpson, J. Osmond, G. Roelkens, J. J. G. M. van der Tol, V. Pruneri, *Appl. Phys. Lett.* **2013**, *103*, 141119.

[14] C. Ríos, M. Stegmaier, P. Hosseini, D. Wang, T. Scherer, C. D. Wright, H. Bhaskaran, W. H. P. Pernice, *Nat. Photonics* **2015**, *9*, 725.

[15] B. Gholipour, J. Zhang, K. F. MacDonald, D. W. Hewak, N. I. Zheludev, *Adv. Mater.* **2013**, *25*, 3050.

[16] M. Wuttig, N. Yamada, *Nat. Mater.* **2007**, *6*, 824.

[17] D. Loke, T. H. Lee, W. J. Wang, L. P. Shi, R. Zhao, Y. C. Yeo, T. C. Chong, S. R. Elliott, *Science (80-.).* **2012**, *336*, 1566.

[18] G. W. Burr, M. J. Breitwisch, M. Franceschini, D. Garetto, K. Gopalakrishnan, B. Jackson, B. Kurdi, C. Lam, L. A. Lastras, A. Padilla, B. Rajendran, S. Raoux, R. S. Shenoy, *J. Vac. Sci. Technol. B* **2010**, *28*, 223.

[19] P. Hosseini, C. D. Wright, H. Bhaskaran, *Nature* **2014**, *511*, 206.

[20] W. H. P. Pernice, H. Bhaskaran, *Appl. Phys. Lett.* **2012**, *101*, 171101.

[21] A. Yariv, *IEEE Photonics Technol. Lett.* **2002**, *14*, 483.

[22] L. Waldecker, T. a. Miller, M. Rudé, R. Bertoni, J. Osmond, V. Pruneri, R. E. Simpson, R. Ernstorfer, S. Wall, *Nat. Mater.* **2015**, *14*, 1.

[23] G. Zhang, F. Gan, S. Lysenko, H. Liu, *J. Appl. Phys.* **2007**, *101*, 033127.

[24] R. L. Cotton, J. Siegel, *J. Appl. Phys.* **2012**, *112*, 123520.

[25] J. Siegel, A. Schropp, J. Solis, C. N. Afonso, M. Wuttig, *Appl. Phys. Lett.* **2004**, *84*, 2250.

[26] Q. Xu, D. Fattal, R. G. Beausoleil, *Opt. Express* **2008**, *16*, 4309.

[27] N. Gruhler, C. Benz, H. Jang, J.-H. Ahn, R. Danneau, W. H. P. Pernice, *Opt. Express* **2013**, *21*, 31678.

[28] C. Ríos, P. Hosseini, C. D. Wright, H. Bhaskaran, W. H. P. Pernice, *Adv. Mater.* **2014**, *26*, 1372.

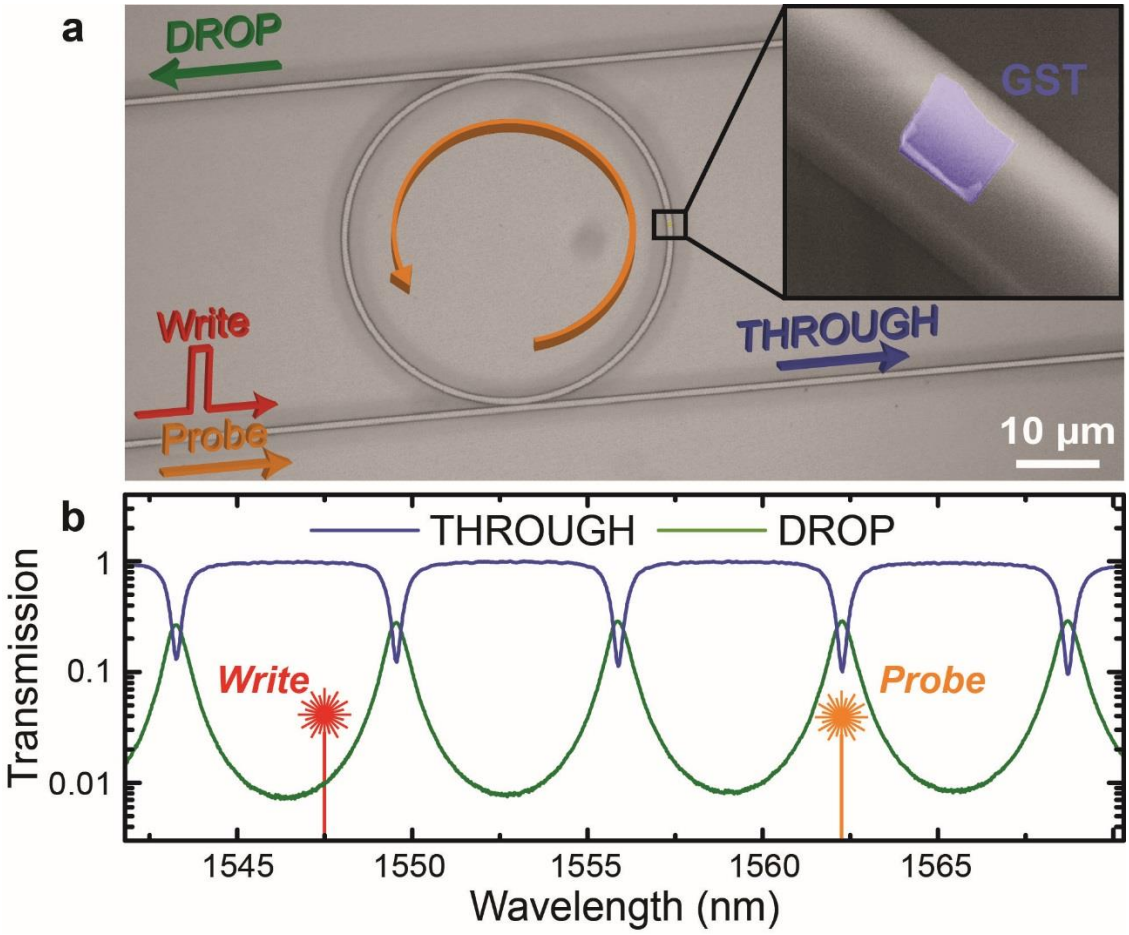

Figure 1. Operation principle of the nonvolatile, all-optical switch. (a) Optical micrograph of the integrated all-optical switch. The GST (inset) is embedded in a ring resonator which is evanescently coupled to two waveguides. (b) Depending on the laser wavelength, all optical power is fully directed to the THROUGH port (off-resonance) or divided between DROP and THROUGH port (on-resonance). Therefore, adjusting the probe signal on-resonance (orange laser symbol) enables control of the light flow by changing the phase-state of the GST and thus the characteristics of the optical cavity.

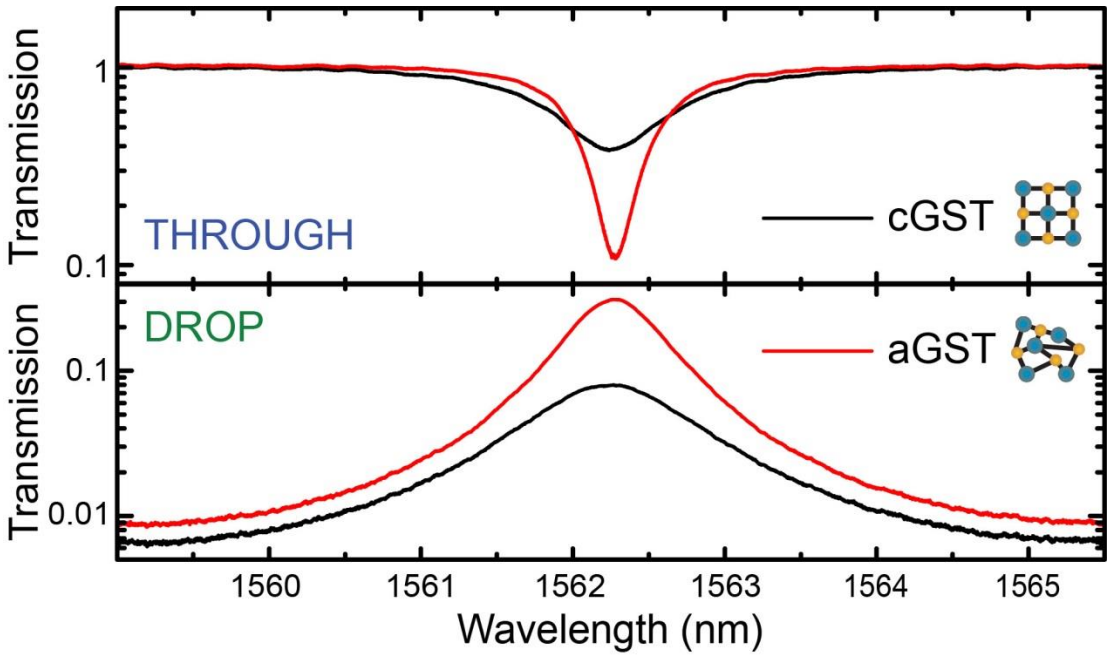

Figure 2. Transmission spectra of the integrated ring resonator in the THROUGH (upper panel) and DROP (lower panel) port for both the crystalline (black traces) and amorphous (red traces) phase of the GST. On-resonance light (1562.3 nm) is directed to the THROUGH port in the crystalline state, but to the DROP port in the amorphous state.

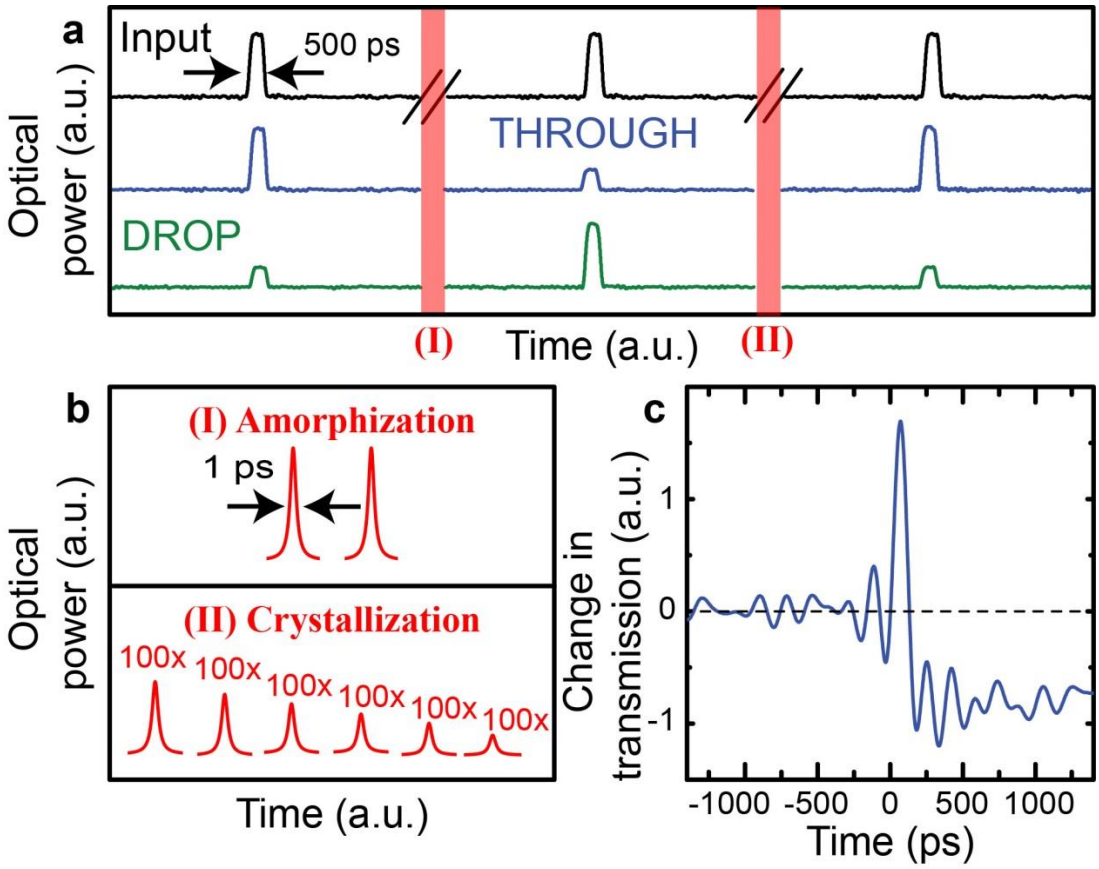

Figure 3. (a) Pulsed probing of the device during one switching cycle. The upper trace shows the probe pulses which are sent into the device while the central and lower trace display the pulses transmitted to the THROUGH and DROP port, respectively. For clarity, the three pulse traces are separately normalized to their respective maximum. (b) Sketch of the pulse sequences used to induce amorphization (upper panel) and crystallization (lower panel). (c) Transient behavior of the probe power transmitted to the THROUGH port during amorphization triggered with a single picosecond pulse at time delay 0 seconds.

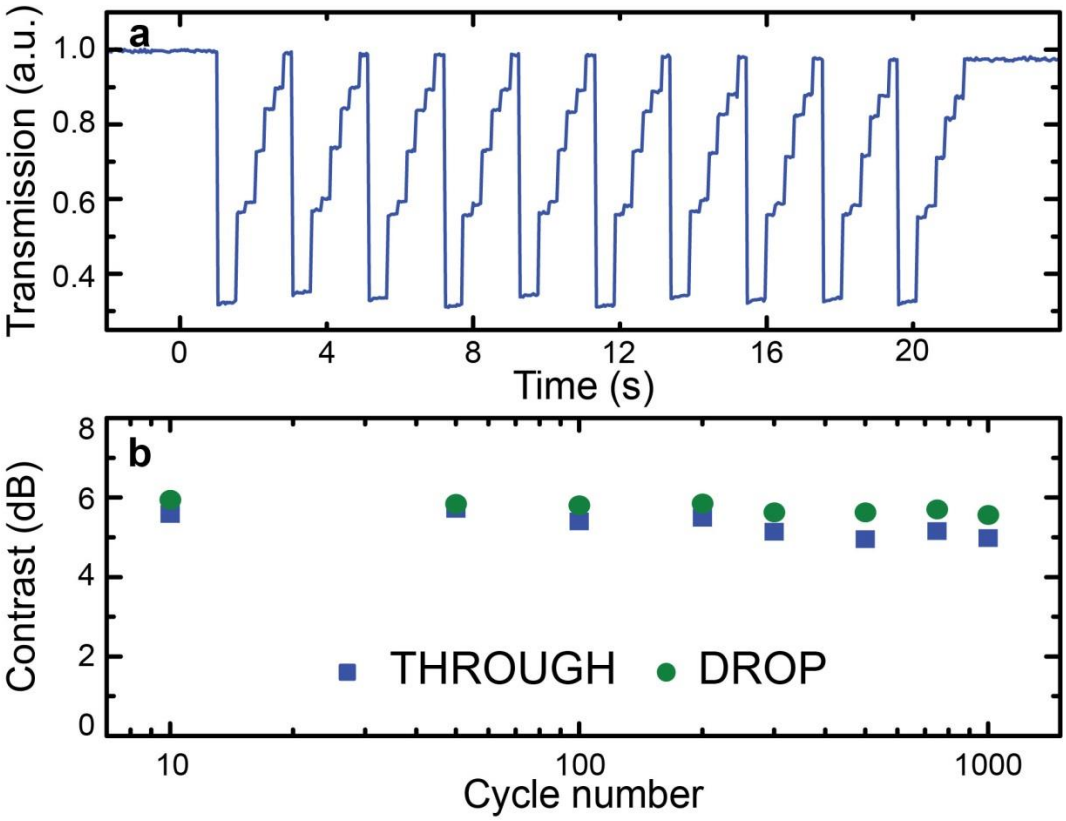

Figure 4. Repeatability test. (a) Transmitted power in the THROUGH port during 10 repetitive switching cycles. As sketched in Figure 3b, one cycle consists of one amorphization and six crystallization steps. (b) The device experiences no significant degradation after 10^3 switching cycles. Here, contrast is defined as the ratio of transmitted power in the on and off-state.